Civil and Environmental Engineering
Vol. 21, Issue 2, 1304-1325, DOI: 10.2478/cee-2025-0096

EFFECT OF CFRP BAR DIAMETER AND CONCRETE STRENGTH ON SHEAR PERFORMANCE OF ETS-STRENGTHENED RC BEAMS WITH RECYCLED PLASTIC AGGREGATE: VALIDATION AND PARAMETRIC STUDY USING ABAQUS

Ahmed Waleed NAQEE[1, *], Raid Ahmed DAUD[2]

[1] Department of Civil Engineering, College of Engineering, University of Technology, Baghdad, Iraq.
[2] Department of Forensic Engineering, Higher Institute of Forensic Sciences, Al-Nahrain University, Baghdad, Iraq.
[*] corresponding author: Ahmadwaleed9711@gmail.com

Abstract

This study investigates the shear performance of sustainable reinforced concrete (RC) beams incorporating recycled plastic aggregate (RPA) and strengthened using the Embedded Through-Section (ETS) technique with carbon fiber-reinforced polymer (CFRP) bars. The experimental program involved twelve beams divided into two groups based on RPA replacement levels (25% and 50%), with variations in CFRP bar orientation (45° and 90°) and placement (edge or centre). All beams were tested under four-point loading with configurations that promote shear-dominated failure modes.
To extend the experimental findings and evaluate broader parametric influences, a comprehensive finite element modelling campaign was conducted using ABAQUS. A total of 54 RC beam models were developed, including 36 models for analysing the effect of CFRP bar diameter and 18 for assessing the impact of concrete compressive strength. The numerical models were calibrated against the experimental data to ensure reliability in simulating shear behaviour, crack development, and load-deflection response.The results demonstrated that increasing the CFRP bar diameter led to a noticeable enhancement in shear capacity, with up to a 28% increase observed in some configurations. However, this improvement was accompanied by a slight reduction in bond efficiency, particularly in beams with lower concrete compressive strength. Increasing concrete strength from 30 MPa to 50 MPa resulted in a stiffness improvement of approximately 22%. Still, it also reduced the effectiveness of aggregate interlock, especially in specimens with 50% recycled plastic aggregate (RPA), where shear strength dropped by up to 15% compared to 25% RPA beams. Among all configurations, the ETS technique was most effective when CFRP bars were installed at a 45° angle and positioned near the beam edges, producing the highest shear resistance and improved crack control. The validated ABAQUS models strongly agreed with experimental results (within 5–8% deviation), confirming their reliability in predicting load-deflection response and failure modes. This integrated experimental-numerical approach offers practical insights for optimizing ETS shear reinforcement strategies in recycled aggregate concrete. It supports the development of sustainable design guidelines for shear-critical RC members.

Keywords:

Embedded Through-Section (ETS);
Finite element analysis;
Recycled plastic aggregate (PVC);
CFRP bars;
Reinforced concrete beams.

1 Introduction

In recent years, the use of advanced composite materials has become increasingly prevalent in structural engineering, particularly in efforts to enhance the durability and extend the service life of reinforced concrete (RC) structures. While RC systems are widely adopted in infrastructure, they are inherently vulnerable to deterioration in aggressive environments, primarily due to the corrosion of embedded steel reinforcement, which accelerates structural degradation and leads to higher maintenance costs [1].

To address these challenges, Fiber-Reinforced Polymer (FRP) composites-especially Carbon Fiber Reinforced Polymer (CFRP)-have emerged as promising alternatives to traditional steel reinforcement. CFRP exhibits exceptional mechanical properties, including high tensile strength, low density, and remarkable corrosion resistance, making it highly suitable for both new construction and structural retrofitting [2]. Additionally, CFRP's non-magnetic and non-conductive properties allow its application in environments sensitive to electromagnetic interference [3].

Among FRP strengthening methods, the Embedded Through-Section (ETS) technique has demonstrated superior effectiveness in enhancing shear capacity. This technique involves drilling through the beam's cross-section and inserting CFRP rods, which are bonded with epoxy to act as internal shear reinforcement [4]. Compared to more conventional methods—such as Externally Bonded Reinforcement (EBR) and Near-Surface Mounted (NSM) systems, the ETS technique offers improved anchorage, enhanced load transfer, and better crack control under shear forces [5].

Despite its proven advantages, the ETS method still presents several unexplored areas, particularly regarding key parameters that govern its effectiveness. For instance, the diameter of CFRP bars plays a crucial role in bond behavior, crack width, and failure mode. While larger bar diameters may enhance stiffness and increase ultimate capacity, they can simultaneously reduce bonding efficiency, especially when embedded in low-strength concrete [6]. Similarly, concrete compressive strength significantly affects load distribution, confinement, and crack propagation. Although higher-strength concrete offers better resistance to cracking, it may reduce aggregate interlock under shear, thereby influencing shear performance [7].

A critical phenomenon closely associated with these factors is the size effect, defined as the reduction in shear strength observed as the member depth increases. This effect is more pronounced in FRP-reinforced systems due to their lower stiffness and reduced dowel action compared to traditional steel reinforcement [8]. Experimental investigations have demonstrated that even well-reinforced FRP-RC beams exhibit notable decreases in shear capacity with increased member depth [9]. The presence of wider cracks, diminished dowel action, and a reduced flexural influence zone further exacerbate this issue in large-scale members [10], particularly those constructed with High-Strength Concrete (HSC), where the depth of the compression zone and aggregate interlock mechanisms are inherently limited [11].

Given the significant financial and logistical demands of large-scale experimental testing, researchers have increasingly turned to Finite Element Analysis (FEA) as a reliable alternative for assessing complex structural behavior. FEA enables detailed simulation of stress distribution, crack initiation and propagation, and nonlinear material interactions [12]. The reliability of these simulations, however, depends heavily on the accuracy of model calibration using experimental data or validated analytical relationships [13].

ABAQUS has become a preferred FEA platform in this field due to its robust nonlinear solvers, comprehensive material libraries, and advanced capabilities for modeling concrete damage plasticity and embedded reinforcements. It has been successfully used to simulate flexural and shear behavior in reinforced concrete members under diverse loading conditions [14]. Nevertheless, existing numerical studies on ETS-strengthened systems remain limited—often focusing on flexural enhancement or traditional steel-RC members—leaving a critical gap in our understanding of how CFRP bar size and concrete strength interact to affect shear capacity in ETS-configured RC elements [15].

Recent developments in FEA have improved the accuracy of such simulations through the adoption of refined mesh densities, softened stress-strain relationships, and carefully calibrated dilation angles to simulate shear-induced cracking [16]. Moreover, by aligning numerical models with experimental outcomes, researchers can significantly improve the predictive capabilities of FEA, reducing reliance on costly full-scale tests and informing the development of more efficient, performance-driven retrofit strategies [17].

Recent studies have reinforced the applicability of CFRP systems in rehabilitating deteriorated or structurally deficient concrete members subjected to diverse loading conditions. For example, [18] evaluated the fatigue performance of damaged RC one-way slabs repaired using CFRP sheets, demonstrating substantial recovery in load capacity and serviceability. [19] investigated the flexural response of corroded RC beams under sustained loading, confirming the long-term benefits of CFRP strengthening.

Similarly, [20] analyzed the behavior of segmental hollow-core slabs under both monotonic and cyclic loads, emphasizing the importance of reinforcement strategies under repetitive stresses. On the numerical side, [21] and [22] applied advanced finite element modeling to assess the performance of hybrid-reinforced and long-term loaded RC components, respectively, validating the predictive accuracy of nonlinear simulations.

These contributions support the present study's focus on experimentally and numerically assessing ETS-CFRP configurations, particularly their interaction with varying bar diameters, concrete strengths, and recycled plastic aggregate content as a means of developing more reliable shear strengthening strategies for sustainable RC structures.

Despite growing interest in CFRP-based strengthening systems, few studies have investigated the combined influence of CFRP bar diameter and concrete compressive strength within the ETS configuration, especially in sustainable concrete made with recycled materials. Most prior research has centered on EBR and NSM techniques, overlooking internal shear reinforcement mechanisms. Additionally, while the size effect in steel-RC members has been explored through numerical methods, limited attention has been given to FRP-reinforced beams with varying shear span-to-depth ratios, bar geometries, and concrete strength levels.

To address these gaps, the present study integrates a comprehensive experimental-numerical approach to evaluate the shear performance of ETS-strengthened beams using CFRP rods and recycled plastic aggregate (RPA). Twelve RC beams were tested, including six with 25% RPA and six with 50% RPA, to investigate the effects of CFRP bar diameter and concrete compressive strength on load capacity, cracking behavior, and failure mode.

The choice of 25% and 50% RPA replacement levels was informed by previous research, which identified these percentages as practical thresholds balancing structural performance and sustainability. The 25% level represents a moderate substitution that maintains acceptable strength, while the 50% level introduces more pronounced reductions in mechanical properties, allowing this study to evaluate ETS effectiveness under increasingly demanding conditions.

The experimental results served as the basis for calibrating a finite element modeling program in ABAQUS, involving 54 RC beam simulations—36 for bar diameter and stirrup configuration, and 18 for concrete strength variation.

The validated finite element models were used for an extended parametric study, enabling deeper insights into the interaction between material properties and geometric parameters. This research provides critical data that can guide the development of more efficient and sustainable ETS retrofitting systems, while also contributing to the understanding of nonlinear shear behavior in recycled concrete structures.

The outcomes of this study carry several practical implications for structural engineers and code committees. Using calibrated FE models reduces the need for full-scale destructive testing, facilitating faster and more economical evaluation of strengthening solutions. Engineers can use the findings to optimize reinforcement strategies tailored to specific strength classes and geometric constraints. Moreover, a better understanding of the bond and size effect mechanisms enables safer design of shear-critical elements in bridges, high-rise structures, and critical infrastructure. Finally, this research lays the groundwork for future design codes incorporating embedded CFRP reinforcement in environmentally sustainable concrete systems.

2 Numerical and experimental work

2.1 Description of the test specimens

The program included twelve rectangular reinforced concrete beams, each measuring 1400 mm in length, 200 mm in width, and 250 mm in depth. The beams were divided into two groups based on the percentage of recycled plastic aggregate (RPA) used as a replacement for coarse aggregate:

- Group 1: Beams with 50% RPA replacement.
- Group 2: Beams with 25% RPA replacement.

Each group consisted of six beams designed to evaluate the effects of ETS-CFRP strengthening configurations and conventional shear reinforcement, as illustrated in Fig. 1. The classification of specimens and corresponding reinforcement details are summarized in Table 1.

Table 1: Details of the tested beams.

No.	Name of beam	Recycled plastic aggregate %	CFRP location	CFRP orientation	Description
1	RPA 25% C	25	/	/	Control without reinforcement in the shear area.
2	RPA 25% C SR	25	/	/	Control with shear reinforcement (5 steel stirrups)
3	RPA 25% 90ϴ E	25	Edge	90	Beam with shear reinforcement (2 bar CFRP)
4	RPA 25% 90ϴ C	25	Centre	90	Beam with shear reinforcement (2 bar CFRP)
5	RPA 25% 45ϴ E	25	Edge	45	Beam with shear reinforcement (2 bar CFRP)
6	RPA 25% 45ϴ C	25	Centre	45	Beam with shear reinforcement (2 bar CFRP)
7	RPA 50% C	50	/	/	Control without reinforcement in the shear area.
8	RPA 50% C SR	50	/	/	Control with shear reinforcement (5 steel stirrups)
9	RPA 50% 90ϴ E	50	Edge	90	Beam with shear reinforcement (CFRP 2 bar)
10	RPA 50% 90ϴ C	50	Centre	90	Beam with shear reinforcement (CFRP 2 bar)
11	RPA 50% 45ϴ E	50	Edge	45	Beam with shear reinforcement (CFRP 2 bar)
12	RPA 50% 45ϴ C	50	Centre	45	Beam with shear reinforcement (CFRP 2 bar)

(A)

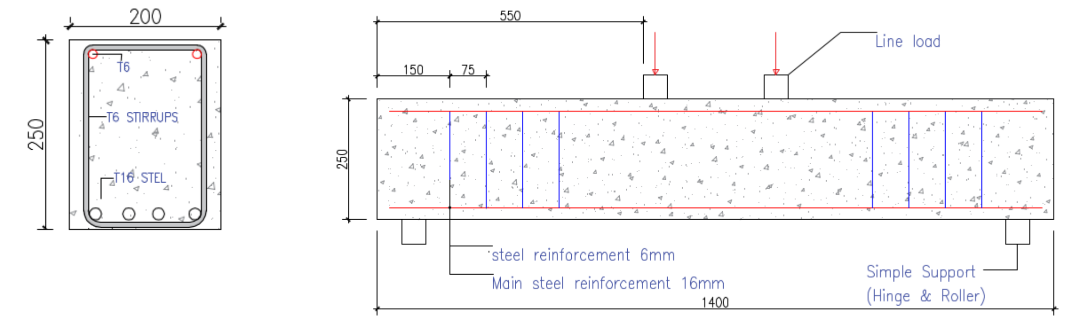

(B)

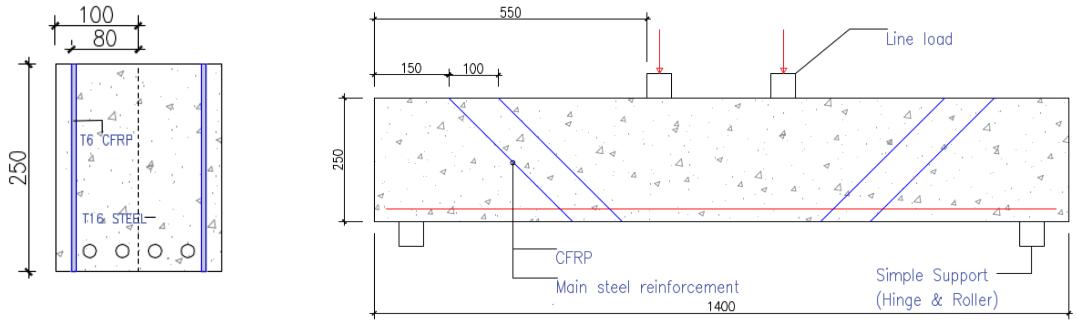

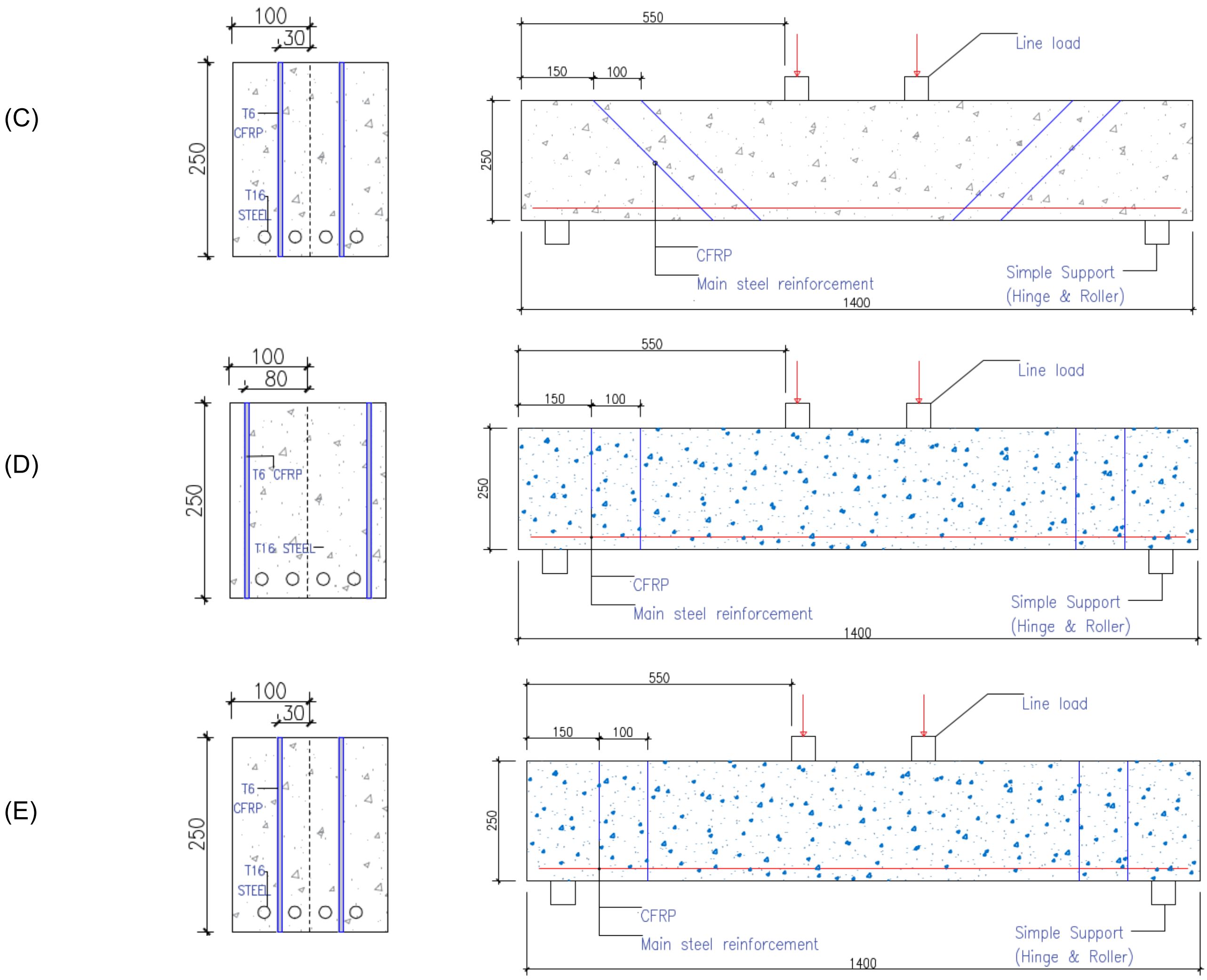

Fig. 1: Dimension and reinforcement details of specimens (A) Steel Strips, (B) CFRP bar in edge with an angle of 45 degrees, (C) CFRP bar in the centre with an angle of 45 degrees, (D) CFRP bar in edge with an angle of 90 degrees, (E) CFRP bar in the centre with an angle of 90 degrees.

2.2 Numerical simulation model

The primary constituents of reinforced concrete (RC) beams reinforced with carbon fibre reinforced polymer (CFRP) are the concrete itself, the steel reinforcement bars embedded inside the concrete, the CFRP bar, and the adhesive layer that connects the CFRP to the RC beams. To accurately represent CFRP-strengthened RC beams subjected to monotonic stress, replicating each component's actual material behaviour is necessary. The ABAQUS physical material library contains material models that accurately simulate the behaviour of all elements.

2.3 Material modelling

2.3.1 Concrete

Two approaches are available in the ABAQUS standard to specify the behaviour of concrete material: smeared cracking and concrete damaged plasticity (CDP). The smeared cracking model characterizes structures such as beams, trusses, solids, and shells. The inquiry in this model does not monitor individual micro-fractures. The damaged plasticity model (CDP) was developed based on the yield function proposed. This approach can accurately represent the behaviour of materials under both compression and tension. The model has two failure mechanisms: tensile cracking and compression fractures. The CDP, or Concrete Damage Plasticity, model is widely recognized for accurately describing concrete behavior. It is particularly useful for nonlinear computations of concrete members, as it offers a comprehensive understanding of how the material behaves (especially in reinforced concrete elements subjected to shear stress).

2.3.2 Steel reinforcement

ABAQUS offers many ways for modelling reinforcement, such as smeared reinforcement within the concrete, cohesive element method, discrete truss or beam elements with the embedded region constraint, or built-in rebar layers. Rebar determines the amounts of uniaxial reinforcement in membrane, shell, and surface elements. The user needs to define one or more levels of reinforcement. For each layer, they should determine the name of the rebar layer, the cross-sectional area of each reinforcement layer, and the spacing of the rebars in the designated plane. This section will focus solely on embedded region modelling, a technique employed for reinforcement modelling in this study. The truss element is a widely used method for modelling reinforcement, requiring simply the input of the cross-sectional area of the bars. Another commonly used structure method is a beam element modelling, which considers the dowel effect and slightly enhances the load-bearing capacity. However, its use is not recommended due to the requirement of defining many input parameters, resulting in a significant computational effort state as the embedded region modelling method does not consider the impact of bond slip. However, the tension-stiffening behaviour of concrete partially incorporates this effect.

2.3.3 Carbon fibre reinforced polymer (CFRP Bar)

The CFRP composite plate was represented as an orthotropic material. It exhibits linear behaviour until it reaches the point of failure. The following equation describes the relationship between stress and strain in CFRP.

$$\begin{bmatrix}\sigma_1\\ \sigma_2\\ \sigma_3\\ \tau_{12}\\ \tau_{13}\\ \tau_{23}\end{bmatrix}=\begin{bmatrix}D_{1111} & D_{1122} & D_{1133} & 0 & 0 & 0\\ & D_{2222} & D_{1212} & 0 & 0 & 0\\ & & D_{3333} & 0 & 0 & 0\\ & & & D_{1212} & 0 & 0\\ & Sym. & & & D_{1313} & 0\\ & & & & & D_{2323}\end{bmatrix}\begin{bmatrix}\varepsilon_{11}\\ \varepsilon_{22}\\ \varepsilon_{33}\\ \gamma_{12}\\ \gamma_{13}\\ \gamma_{23}\end{bmatrix} \quad \text{……………………………….(1)}$$

$D1111 = E1(1 - \nu 23 \nu 32)\,\gamma$ ……………………………………………………………………….(2)
$D2222 = E2(1 - \nu 13 \nu 31)\,\gamma$ ……………………………………………………………………….(3)
$D3333 = E3(1 - \nu 12 \nu 21)\,\gamma$ ……………………………………………………………………….(4)
$D1122 = E1(\nu 21 - \nu 31 \nu 23)\,\gamma = E2\,(\nu 12 - \nu 32 \nu 13)\,\gamma$ ……………………………………………….(5)
$D1133 = E1(\nu 31 - \nu 21 \nu 32)\,\gamma = E3(\nu 13 - \nu 12 \nu 23)\,\gamma$ ……………………………………………….(6)
$D2233 = E2(\nu 32 - \nu 12 \nu 31)\,\gamma = E3(\nu 23 - \nu 21 \nu 13)\,\gamma$ ……………………………………………….(7)
$D1212 = G12,\ D1313 = G13,\ D2323 = G23$ ……………………………………………………….(8)
$\gamma = \frac{1}{1-\nu 12\nu 21-\nu 23\nu 32-\nu 31\nu 13-2\nu 21\nu 32\nu 13}$ ……………………………………………………….(9)

2.4 Main meshing elements

The finite element model was developed using ABAQUS, employing two element types to represent different components of the reinforced concrete beams. The concrete domain was meshed using 8-node linear brick elements (C3D8R), while the internal steel reinforcement and CFRP bars were modelled using 2-node truss elements (T3D2).

The mesh sensitivity analysis was conducted using element sizes of 30 mm, 40 mm, and 50 mm. Based on a comparison with experimental results, the 30 mm mesh provided the best accuracy in capturing load-deflection behaviour and crack propagation and was therefore adopted for all models. Fig. 2 illustrates the full mesh configuration used in the analysis. Fig. 2 shows the whole model with mesh.

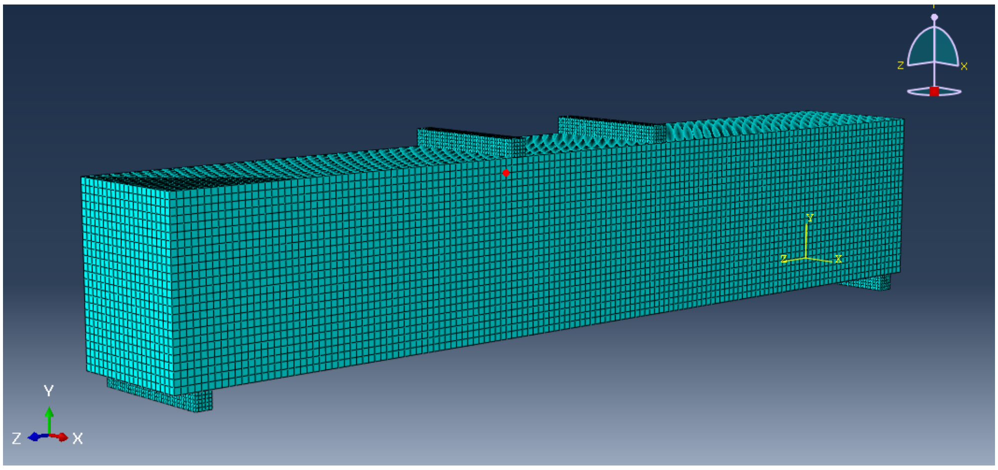

Fig. 2: Mesh for Abaqus model.

2.5 Boundary conditions

Defining the boundary conditions accurately was a key aspect of the finite element modelling in ABAQUS. The beam was modelled as supported, with one end restrained in both the X and Y directions and the other restrained only in the Y direction. Rectangular support plates (25 × 25 × 200 mm) were added under both ends to simulate real support conditions. A tie constraint was used to model the interaction between the support plates and the concrete. Fig. 3 shows the support configuration and boundary conditions.

2.6 Loads

The Static General procedure in ABAQUS was used to apply the monotonic loading on the beam. Loading was introduced as a pressure on the top surface of rectangular steel plates placed at two points along the beam. Each loading plate measured 25 × 25 × 200 mm, consistent with the experimental setup. The load was distributed across a concrete contact width of 25 mm, simulating the line load applied in the physical test. The tie constraint fully bonded the load plates to the concrete surface, ensuring uniform stress transfer without slippage. Fig. 3 shows the loading configuration used in the finite element model.

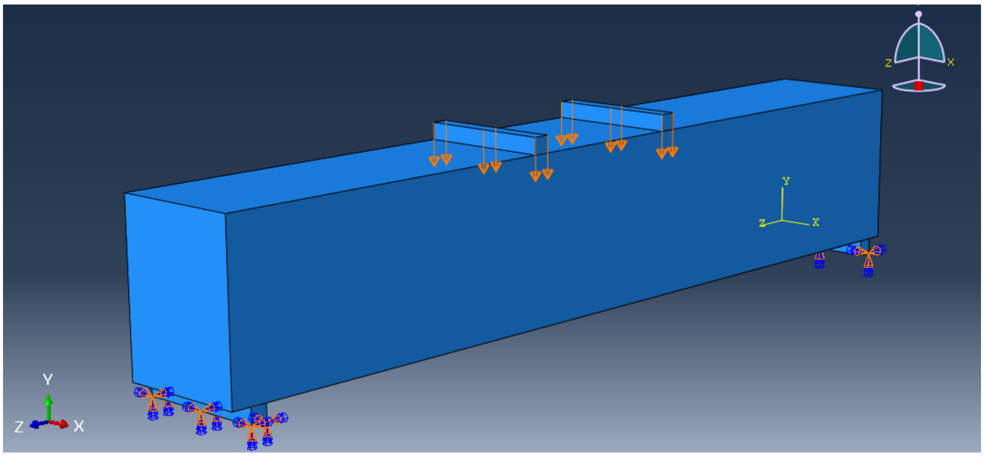

Fig. 3: Specification of loading line as pressure on beams in ABAQUS.

2.7 Finite element model and input data

The numerical specimen was modelled using the general finite element software package ABAQUS 6.13. Tables 2 and 3 present the concrete compressive and tensile strengths based on experimental results and other necessary parameters such as eccentricity, dilation angle, ϵbo=ϵco, kc, and viscosity. The default values provided by ABAQUS were used for these parameters. Tables 4 and 5 also summarize the input data for the concrete plasticity and CFRP material properties, respectively.

In ABAQUS, the concrete beam was modelled using an 8-node linear brick element (C3D8R) to represent the concrete part, while a 2-node truss element (T3D2) was employed for the CFRP bars and the steel reinforcement. The steel reinforcement was embedded within the concrete to ensure a full bond between the concrete and the steel. Similarly, the CFRP bars were embedded inside the concrete to simulate a complete bond between the CFRP and the surrounding concrete.

Table 2: Concrete compressive strength.

Yield Stress [MPa]	Inelastic strain [με]
17.18	0.000604
21.03	0.000768
21.9	0.000809
23.25	0.000878
25.58	0.001015
29.54	0.001425
30	0.001642
29.63	0.001806
28.7	0.001970
27.42	0.002135
25.69	0.002299

Table 3: Concrete tension data.

Yield Stress [MPa]	Strain [με]
2.31	0.0000258
1.96	0.0000547
1.67	0.0000818

Table 4: Input data for concrete.

Data	Value
Poisson ratio	0.2
Dilation angle	36
Eccentricity	0.1
ϵbo/ϵc	1.16
kc	0.667
Viscosity parameter	0.001

Table 5: Properties of CFRP bar.

Data	Value
D1111	168408.2
D1122	6511.7
D2222	17851.27
D1133	5838.15
D2233	4625.61
D3333	17801.85
D1212	6894
D1313	6894
D2323	4136.8

3 Comparison between the shear beam test's numerical Model and Experimental Results

The load-displacement (mid-span displacement) curves obtained from the FE models were compared with experimental results for the six tested beams (three with 25% RPA and three with 50% RPA), as shown in Fig. 4 (A–F). Each subfigure illustrates the comparison for a specific beam configuration, including control, steel-stirrup-reinforced, and ETS-CFRP-strengthened beams. Table 6 presents the percentage difference between the maximum experimental and FE-predicted load and deflection values.

The crack patterns observed in both experimental and numerical analyses for the CFRP-strengthened beams were largely similar across six beams, as shown in Fig. 5 (A-F), with only minor load and deflection values that did not significantly alter the failure mode or overall crack distribution.

Table 6: Comparisons between the maximum experimental and FE load and deflection.

Name of beam	Excremental Load [kN]	Numerical Load [kN]	Difference [%] (Load)	Excremental Def. [mm]	Numerical Def. [mm]	Difference [%] (Def.)
RPA 25% C	144	158.85	10.3	43	38.5	10.33
RPA 25% C SR	261	271.46	4	60	64.1	6.78
RPA 25% 90ϴ C	200	217.908	8.95	59.7	58.74	1.6
RPA 25% 90ϴ E	243.34	252.256	3.66	64	61.67	3.62
RPA 25% 45ϴ C	264.5	264.89	0.13	72	71.39	0.83
RPA 25% 45ϴ E	287.104	306.619	6.79	78	74.9	3.9
RPA 50% C	120.212	125.67	4.54	40	39.6	1
RPA 50% C SR	230	245.236	6.62	64	58.27	8.94
RPA 50% 90ϴ C	170	179.27	5.45	49.8	46.61	6.43
RPA 50% 90ϴ E	220	219.67	0.149	53.4	53.84	0.834
RPA 50% 45ϴ C	230	230.655	0.28	64.95	65.3	0.52
RPA 50% 45ϴ E	267	276.786	3.6	74	65.3	11.7

The discrepancy between the experimental and FE-predicted deflections arises primarily from the measurement method. In the experimental setup, the deflection was recorded directly using an LVDT. In contrast, in the numerical model, displacement was extracted from the mid-span of the beam in the FE simulation.

The FE models exhibited significantly higher stiffness compared to experimentally tested beams. Several key factors contribute to this discrepancy:

1. Pre-existing microcracks: Minor cracks may develop in the concrete before testing during specimen preparation, transportation, or due to drying shrinkage. These pre-existing cracks contribute to reduced stiffness in experimental beams. However, ABAQUS does not account for such microcracks, leading to an overestimating stiffness in the FE models.
2. Bond assumptions: In real experimental conditions, the interaction between reinforcement bars and concrete introduces slip and localized debonding, reducing the overall rigidity of the system. In contrast, FE models often assume a perfect bond between CFRP and concrete, which leads to higher predicted stiffness.

These factors collectively result in differences between experimental and numerical load-deflection responses.

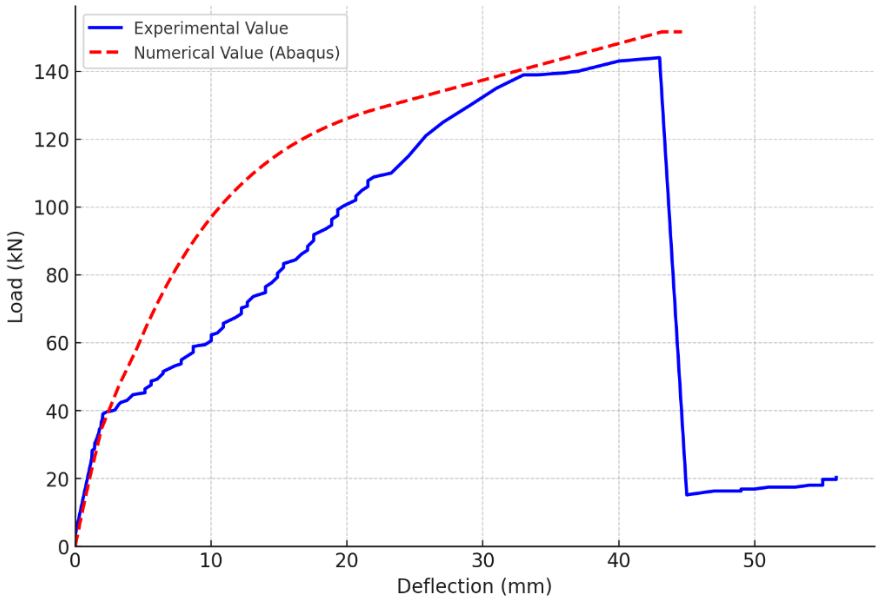

Fig. 4A. Load–deflection curve of control beam with 25% recycled plastic aggregate (RPA).

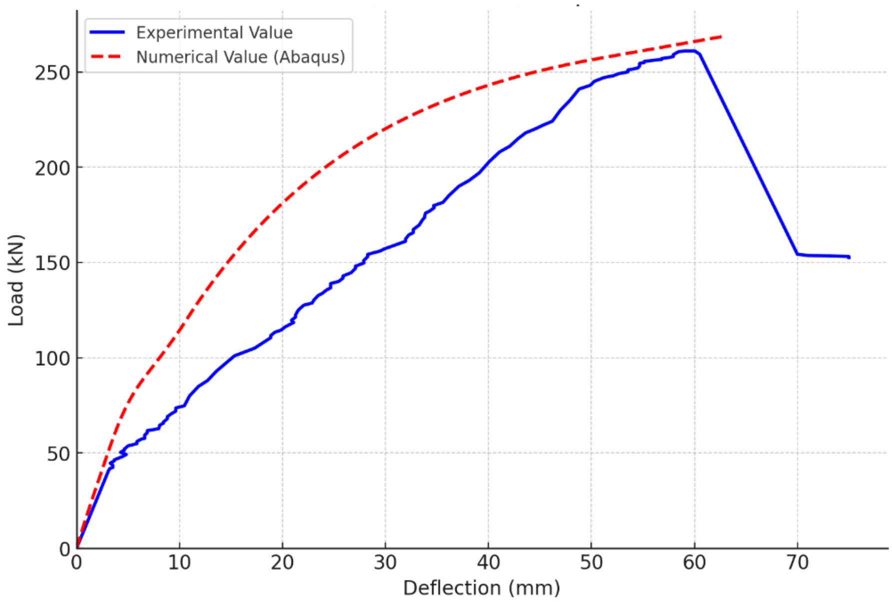

Fig. 4B: Load–deflection curve of beam with steel stirrups and 25 % RPA.

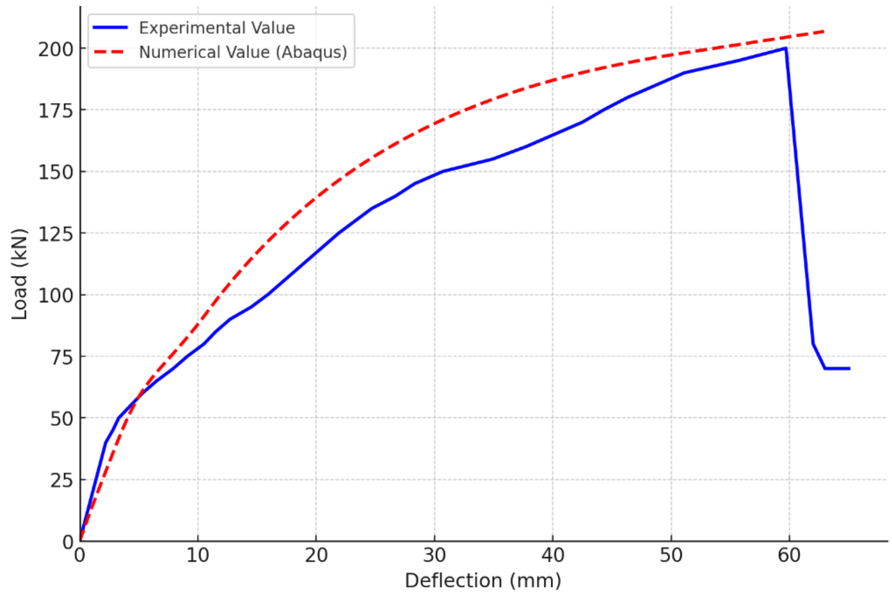

Fig. 4C: Load–deflection curve of beam with vertical ETS-CFRP bars (90°, center) and 25 % RPA.

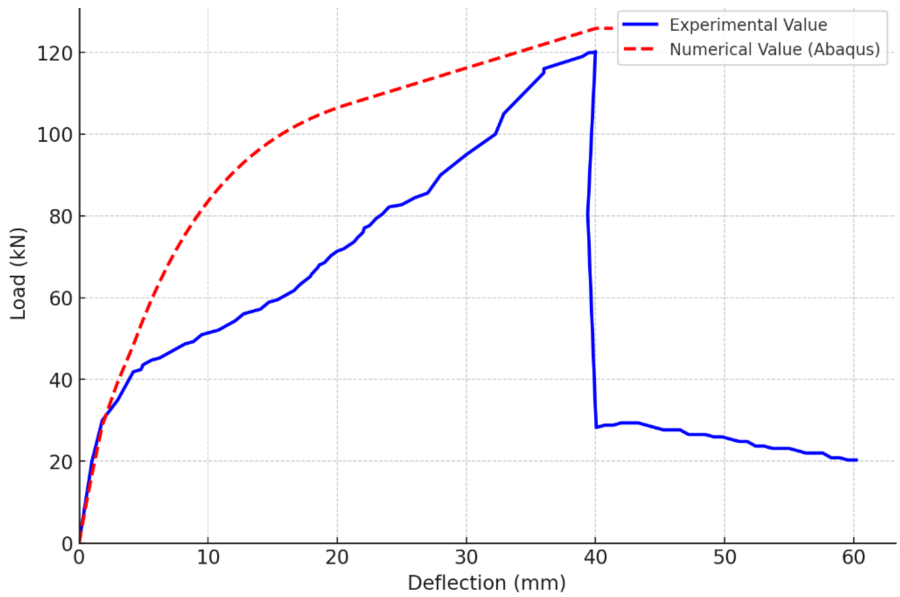

Fig. 4D: Load–deflection curve of control beam with 50 % RPA.

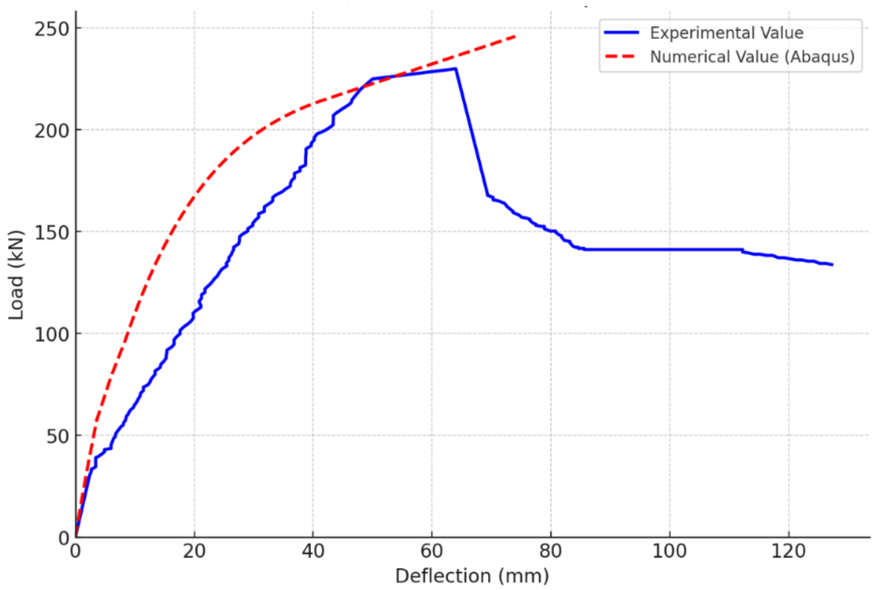

Fig. 4E. Load–deflection curve of beam with steel stirrups and 50% RPA.

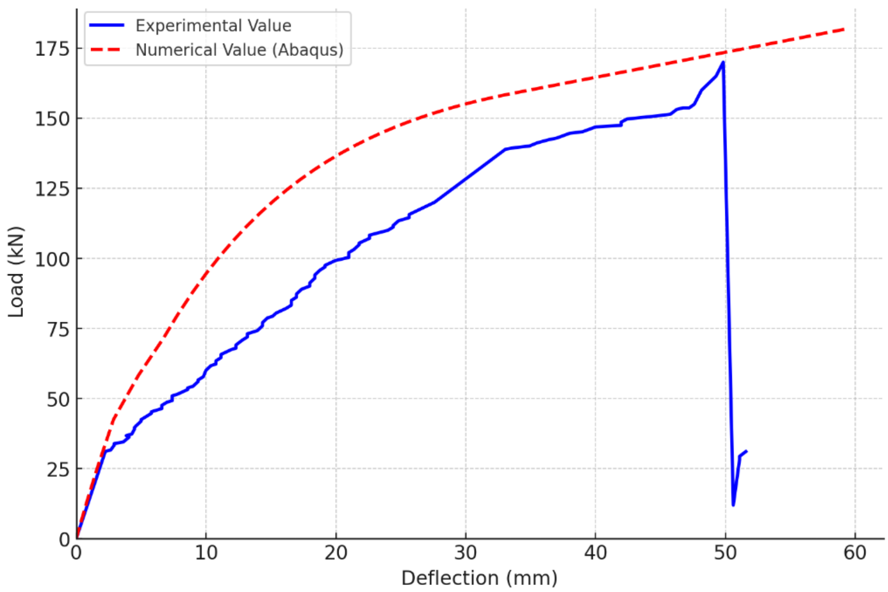

Fig. 4F. Load–deflection curve of beam with vertical ETS-CFRP bars (90°, center) and 50% RPA.

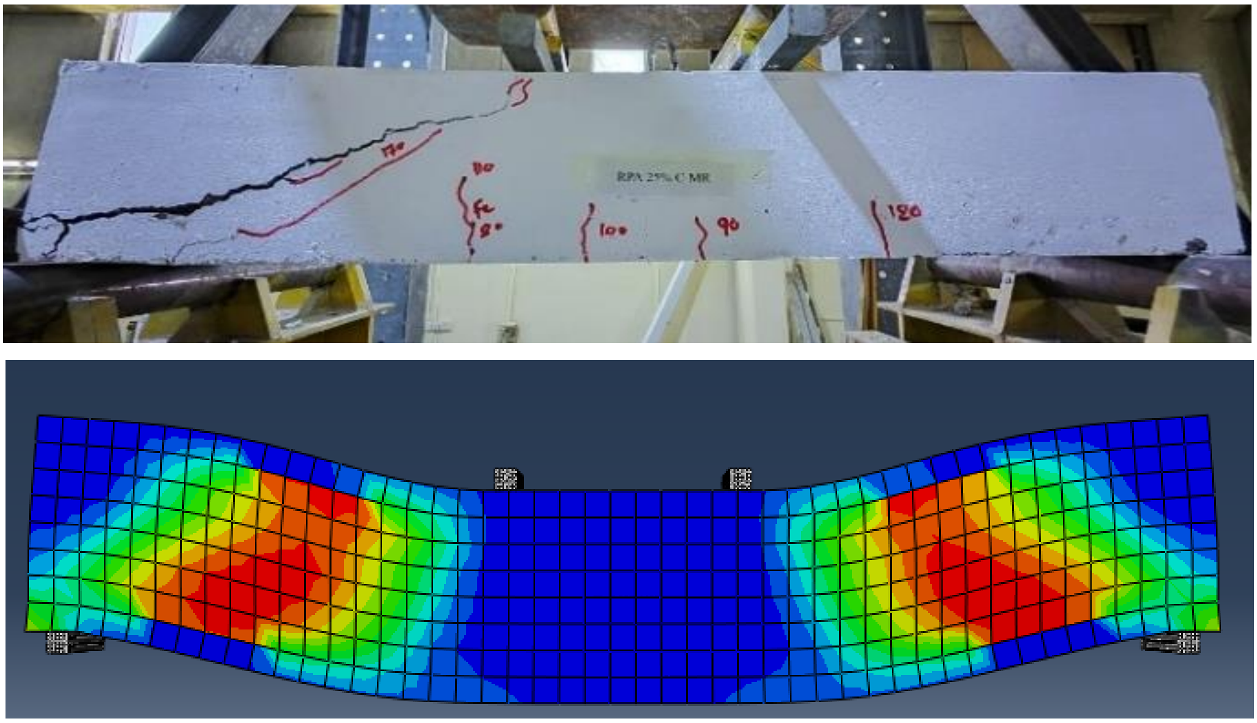

Fig. 5A. Failure mode (experimental vs. numerical) of control beam with 25% recycled plastic aggregate (RPA).

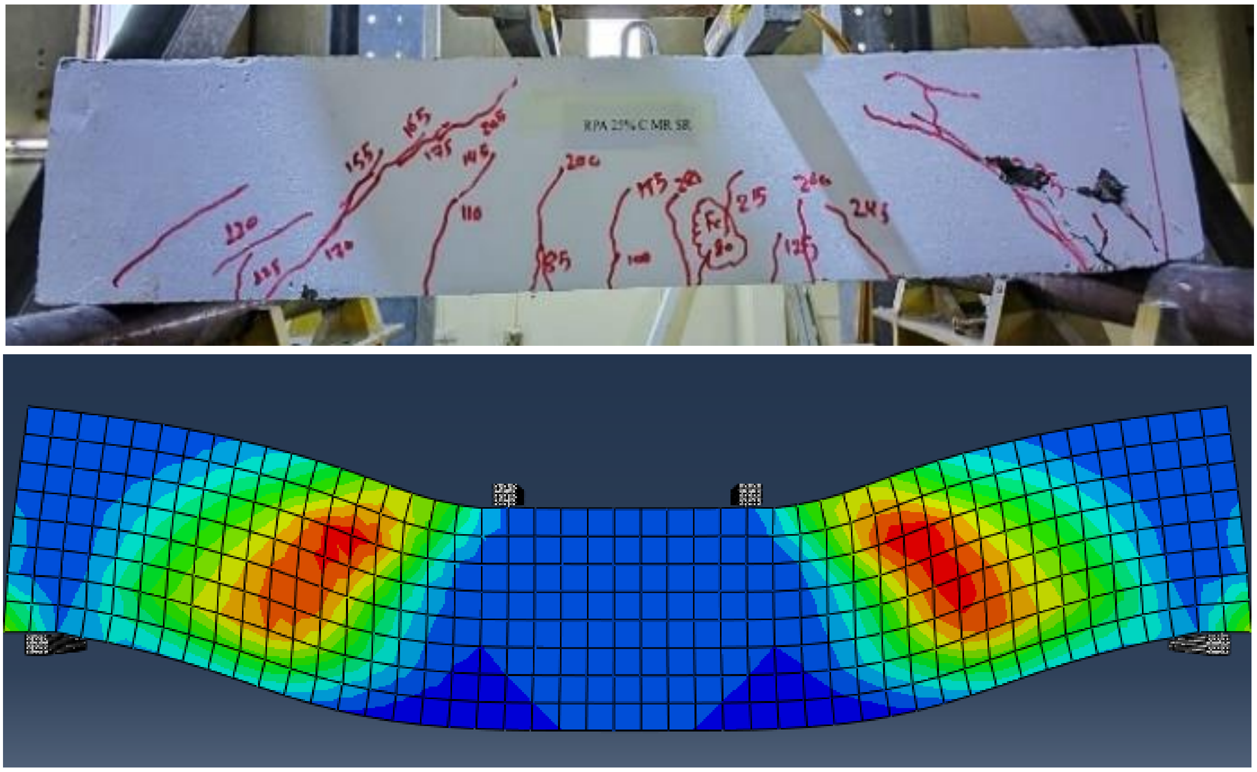

Fig. 5B. Failure mode (experimental vs. numerical) of beam with steel stirrups and 25% RPA.

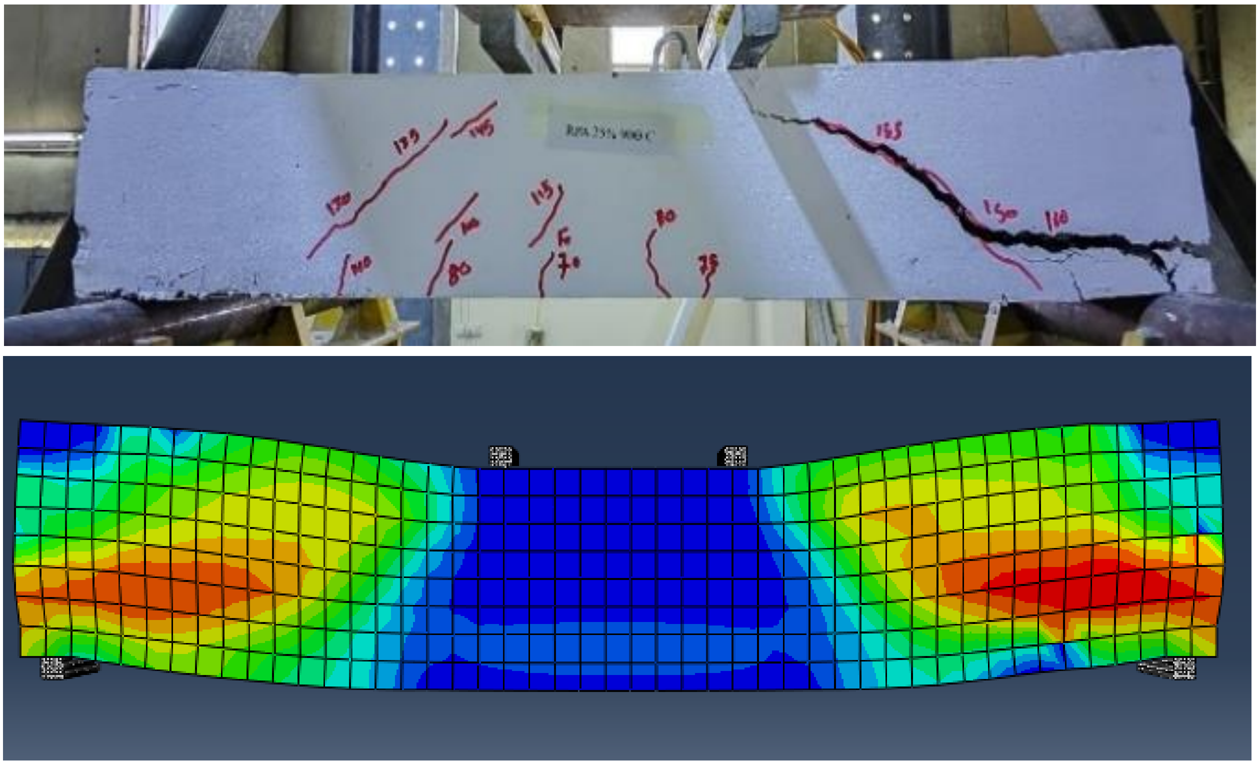

Fig. 5C. Failure mode (experimental vs. numerical) of beam with vertical ETS-CFRP bars (90°, center) and 25% RPA.

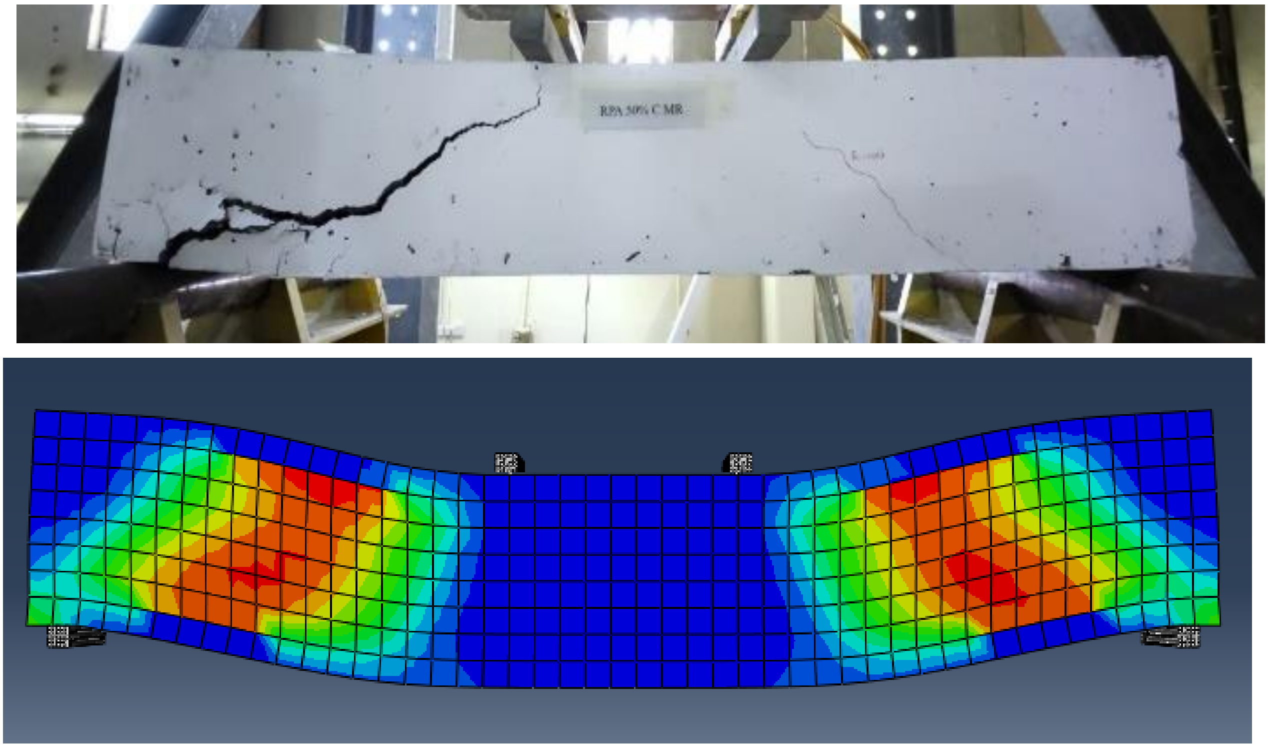

Fig. 5D. Failure mode (experimental vs. numerical) of control beam with 50% RPA.

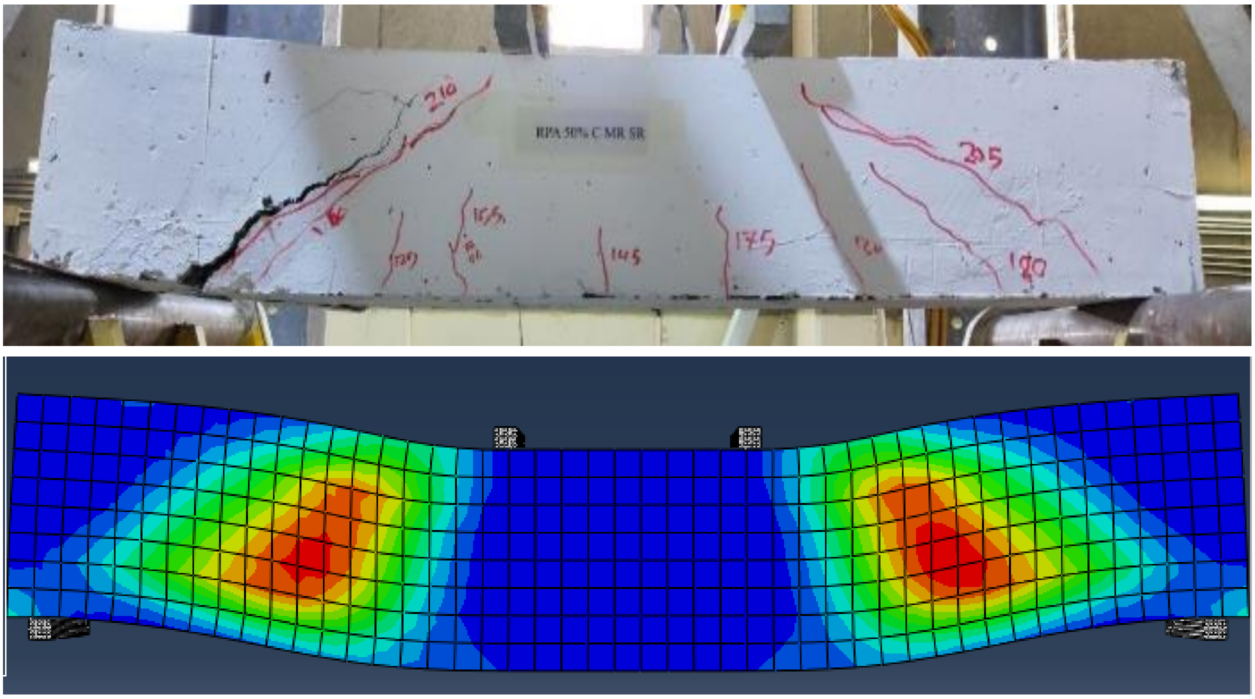

Fig. 5E. Failure mode (experimental vs. numerical) of beam with steel stirrups and 50% RPA.

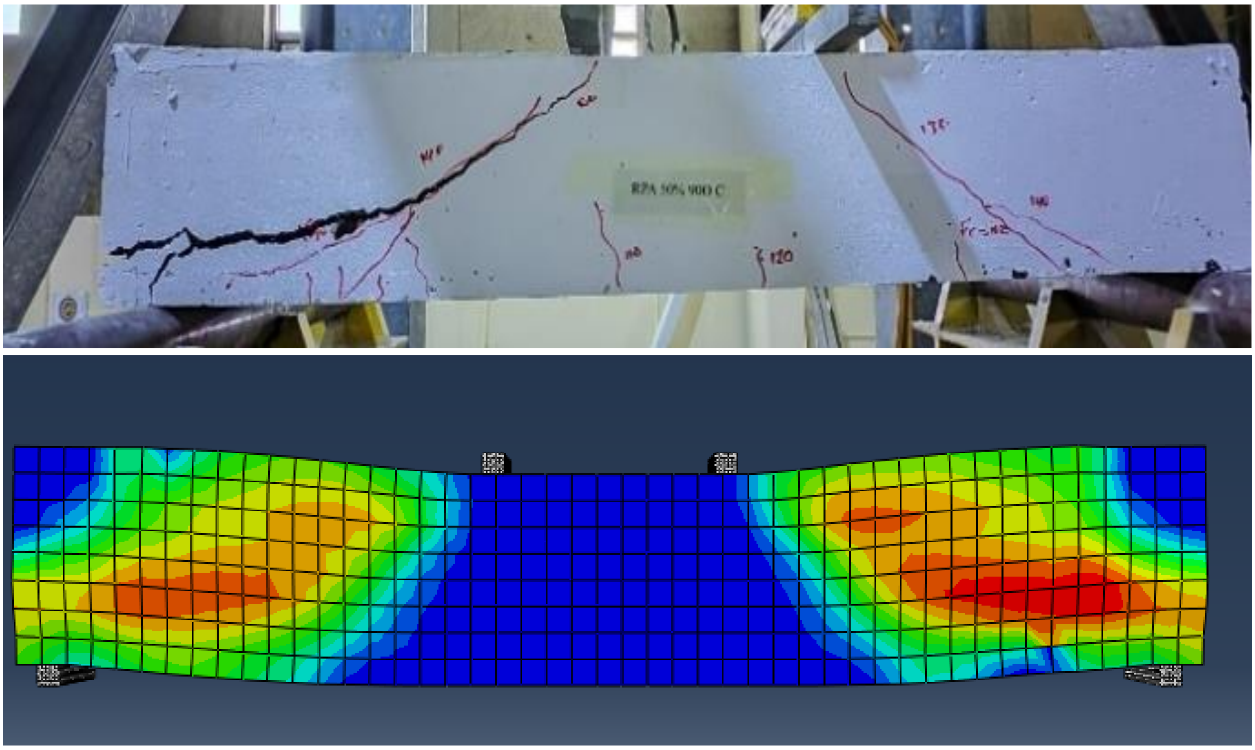

Fig. 5F. Failure mode (experimental vs. numerical) of beam with vertical ETS-CFRP bars (90°, center) and 50% RPA.

The comparison in Fig. 5 (A-F) demonstrates a strong agreement between experimental crack patterns and the numerical damage contours predicted by ABAQUS for various beam configurations. In both 25% and 50% RPA groups, the control beams exhibited pronounced diagonal shear cracks originating near the supports, indicative of brittle shear failure - a behaviour successfully replicated in the simulations. Beams with steel stirrups showed more distributed and narrower cracks experimentally, while the numerical models exhibited similar damage spread with slightly reduced intensity. ETS-strengthened beams with vertical CFRP bars exhibited improved crack confinement around the anchorage zones and limited crack propagation across the shear span, closely matching the numerical damage zones.

The percentage difference in maximum load between experimental and FE results ranged from 0.13% to 10.3%, while deflection differences ranged from 0.52% to 11.7% across all configurations. These deviations are within acceptable engineering tolerances and did not significantly alter the observed failure modes or crack distributions. The slightly higher stiffness observed in the FE models is attributed to idealized modelling assumptions, such as the absence of pre-existing microcracks and the use of perfect bond conditions between concrete and reinforcement. Despite these simplifications, the crack orientation, failure zone location, and overall shear behaviour were highly consistent, confirming the validity of the numerical model in simulating ETS-strengthened RC beams.

3 Results and dissection

The experimental program evaluated the structural behaviour of twelve reinforced concrete beams with varying configurations. The key parameters investigated included the percentage of plastic aggregate replacement (25% and 50%), the inclination angle of ETS (Embedded Through-Section) CFRP bars (90° and 45°), and their placement location (centre and edge). The load-deflection response, failure modes, and strain behaviour were analysed to assess the influence of these parameters on shear capacity and overall beam performance. The numerical simulation model confirmed in this section has been used to study the behaviour of the CFRP strengthening beam by changing the following different parameters: CFRP bar diameters (6, 8, and 10) mm and Concrete compressive strength (30, 40, and 50 MPa), as shown in Tables 7 and 8.

Table 7: Summary of the Numerical load results (peak load in kN).

	Bar diameter			Concrete compressive strength		
Name of beam	**6 [mm]**	**8 [mm]**	**10 [mm]**	**30 [MPa]**	**40 [MPa]**	**50 [MPa]**
RPA 25% C	/	/	/	125.67	142.96	158.85
RPA 25% C SR	271.46	339.32	366.47	245.23	256.55	271.46
RPA 25% 90Ɵ C	217.90	272.38	294.17	179.27	209.19	217.90
RPA 25% 90Ɵ E	252.25	315.32	340.54	219.67	227.03	252.25
RPA 25% 45Ɵ C	264.86	331.08	357.57	230.65	246.32	264.86
RPA 25% 45Ɵ E	306.61	383.27	413.93	276.78	285.15	306.61
RPA 50% C	/	/	/	125.67	142.96	158.85
RPA 50% C SR	245.23	294.28	323.71	245.23	256.55	271.46
RPA 50% 90Ɵ C	179.27	215.12	246.58	179.27	209.19	217.90
RPA 50% 90Ɵ E	219.67	263.60	289.96	219.67	227.03	252.25
RPA 50% 45Ɵ C	230.65	276.78	325.16	230.65	246.32	264.86
RPA 50% 45Ɵ E	276.78	332.14	365.35	276.78	285.15	306.61

Table 8: Summary of the numerical deflection results (maximum deflection in mm).

	bar diameter [mm]			Concrete compressive strength [MPa]		
Name of beam	**6 [mm]**	**8 [mm]**	**10 [mm]**	**30 [MPa]**	**40 [MPa]**	**50 [MPa]**
RPA 25% C	/	/	/	39.6	38.55	38.55
RPA 25% C SR	64.10	73.71	76.92	58.27	58.97	64.10
RPA 25% 90ϴ C	58.74	67.55	70.48	46.61	55.80	58.74
RPA 25% 90ϴ E	61.67	70.92	74.01	53.84	55.50	61.67
RPA 25% 45ϴ C	71.39	82.10	85.67	65.30	66.40	71.39
RPA 25% 45ϴ E	74.96	86.21	89.96	65.80	69.72	74.96
RPA 50% C	/	/	/	39.6	38.55	38.55
RPA 50% C SR	58.27	64.10	67.01	58.27	58.9	64.10
RPA 50% 90ϴ C	46.61	51.28	53.61	46.61	55.80	58.74
RPA 50% 90ϴ E	53.84	59.22	61.92	53.84	55.50	61.67
RPA 50% 45ϴ C	65.30	71.83	75.09	65.30	66.40	71.39
RPA 50% 45ϴ E	65.80	72.63	75.89	65.80	69.72	74.96

3.1 Effect of increasing bar diameter for steel and CFRP

Fig. 6 and 7 illustrate the influence of bar diameter on the load-carrying capacity and displacement of reinforced concrete beams incorporating 25 % and 50% plastic aggregate replacement. The results demonstrate that increasing the bar diameter from 6 mm (experimental data) to 8 mm and 10 mm (numerical simulation) improves load-carrying capacity across all reinforcement configurations. For instance, the load in 25 % replacement beams increased from 306.6 kN at 6 mm to 413.9 kN at 10 mm for the ETS-CFRP 45° E, representing a 35 % gain. Steel reinforcement also showed significant improvement, with loads rising from 271.5 kN to 366.4 kN across the same bar size increase. However, CFRP-reinforced beams consistently outperformed their steel counterparts at all diameters.

A pronounced difference is observed between the two levels of plastic aggregate replacement: beams with 50 % replacement consistently display reduced load capacity. For example, the maximum load recorded for the 50 % ETS-CFRP 45° E was 365.3 kN, nearly 12% lower than the corresponding 25% case. This reduction highlights the weakening effect of higher plastic content on the concrete matrix, limiting its ability to effectively transfer shear and flexural stresses.

Regarding deflection behaviour, increasing the bar diameter results in a corresponding increase in displacement across all configurations, particularly in beams reinforced with ETS-CFRP at 45°. In the 25 % group, deflection rose from 74.9 mm at 6 mm diameter to 89.9 mm at 10 mm, while in the 50% group, it reached 75.9 mm-again illustrating the influence of plastic content. In contrast, beams with steel stirrups showed lower deflection ranges, between 64.1 mm and 76.9 mm for 25% plastic aggregate and 58.3 mm to 67.0 mm for 50 %.

Despite higher load capacity, ETS-CFRP edge-reinforced beams exhibited larger deflections, indicating a trade-off between strength and stiffness. For example, comparing ETS 45° edge and steel SR beams at 10 mm, the deflection was approximately 17% higher in the CFRP-reinforced beam despite its 13 % greater load. This suggests that while CFRP reinforcement is more effective in carrying load, it introduces slightly more flexibility into the system. These results emphasize the importance of balancing reinforcement type, bar size, and plastic aggregate content to optimize strength and ductility in structural performance.

(A)

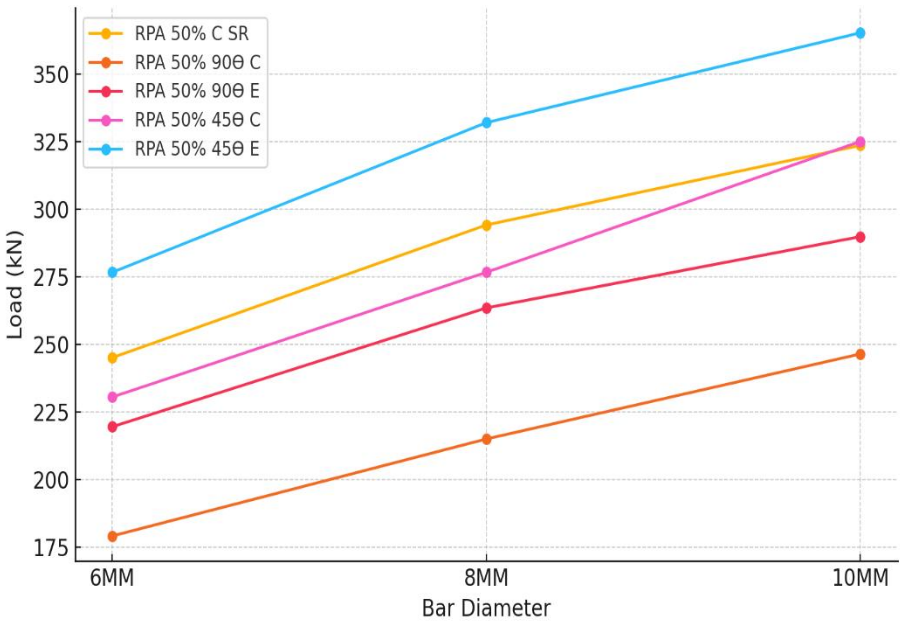

(B)

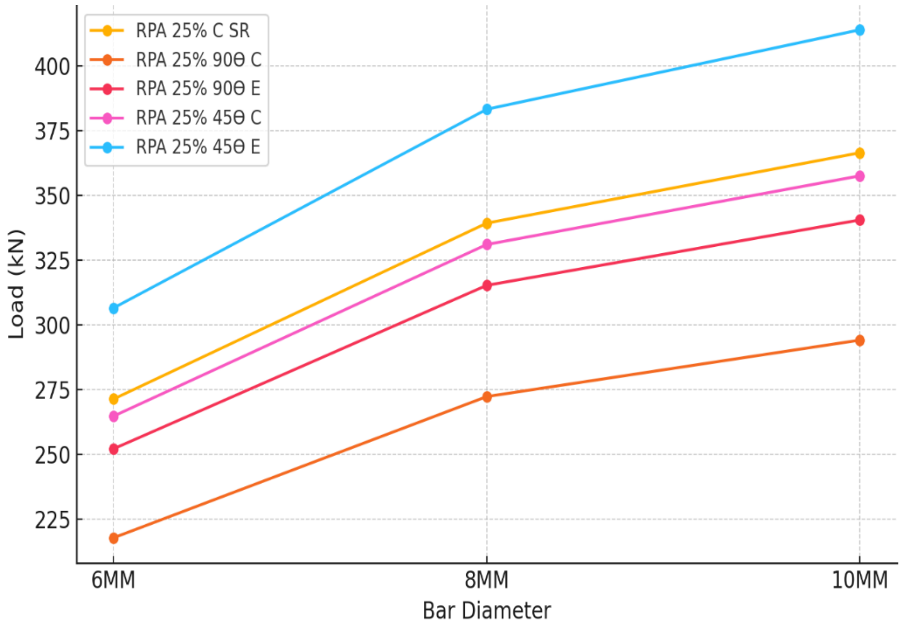

Fig. 6: Effect of bar diameters on load-carrying capacity (A 50%, B 25%).

(A)

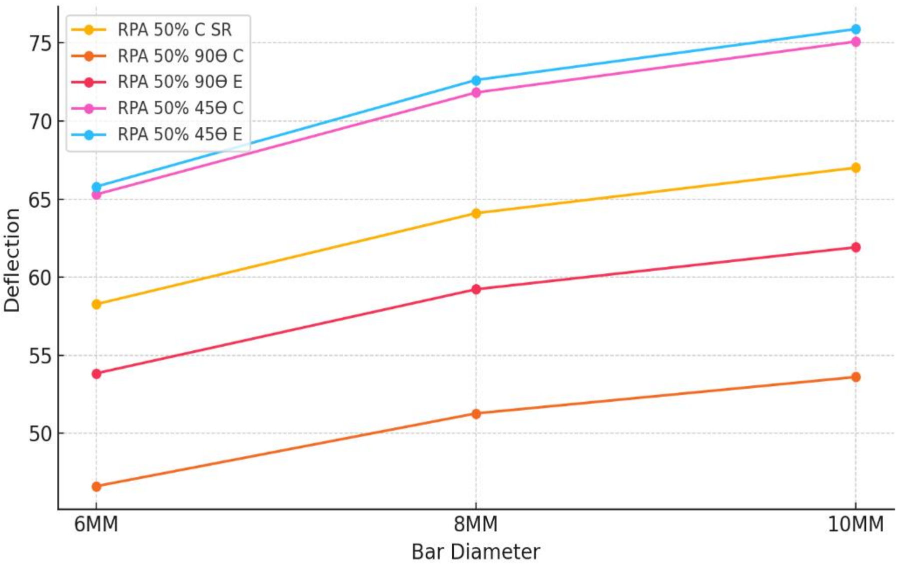

(B)

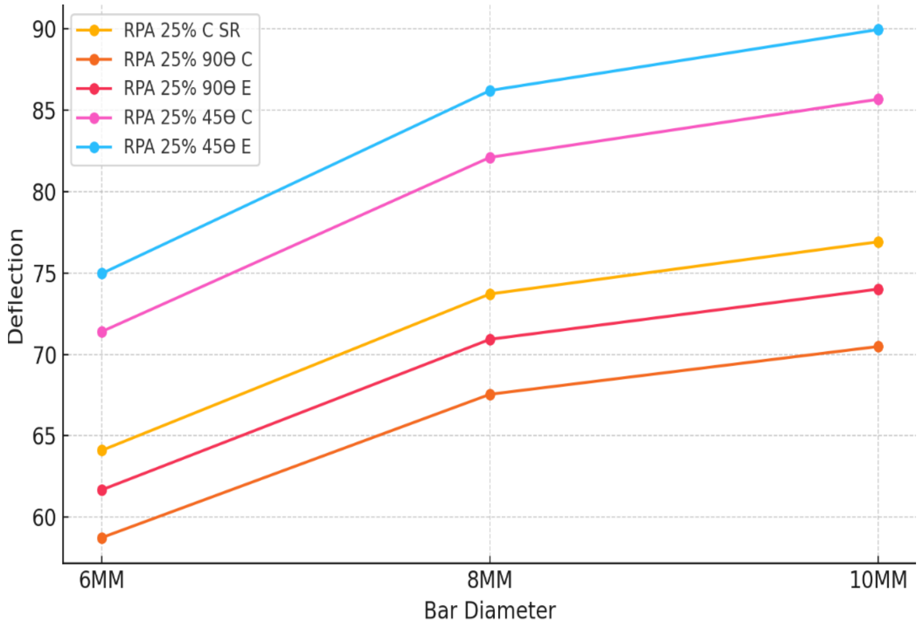

Fig. 7: Effect of bar diameters on deflection value (A 50%, B 25%).

3.2 Effect of increasing concrete compressive strength

Fig. 8 and 9 illustrate the effect of increasing concrete compressive strength on the load-carrying capacity and displacement behavior across various reinforcement configurations. As the compressive strength increases from 30 MPa to 50 MPa, a consistent enhancement in load-bearing capacity is observed for all reinforcement types. For instance, the ETS-CFRP beam with 45° edge placement reached a peak load of 306.6 kN at 50 MPa, compared to 276.8 kN at 30 MPa, marking an approximate 11 % increase. Similarly, steel-reinforced beams (C SR) increased from 245.2 kN to 271.5 kN, while centrally placed 90° CFRP reinforcement improved from 179.3 kN to 217.9 kN over the same strength range. In contrast, the control beam without shear reinforcement increased from 125.7 kN to 158.9 kN, remaining the lowest performer across all strengths. These results underscore the clear advantage of shear reinforcement and the added efficiency of ETS-CFRP systems, especially when used at optimal angles and positions.

On the other hand, displacement behavior presents a more varied trend with increasing compressive strength. While steel-reinforced beams (C SR) showed relatively controlled deflections, ranging from 58.3 mm at 30 MPa to 64.1 mm at 50 MPa, ETS-CFRP beams with 45° edge placement exhibited more noticeable increases, from 65.8 mm to 74.9 mm - an increase of nearly 14 %. Interestingly, despite its poor load performance, the control beam exhibited the lowest deflection overall at 38.6 mm, indicating a brittle failure mode rather than true structural stiffness. This contrast highlights how higher concrete strength can enhance stiffness and redistribute stress more aggressively within well-reinforced beams, potentially leading to greater flexibility in certain configurations. These findings show that the interaction between concrete compressive strength, reinforcement type, and positioning significantly influences load capacity and deformation characteristics.

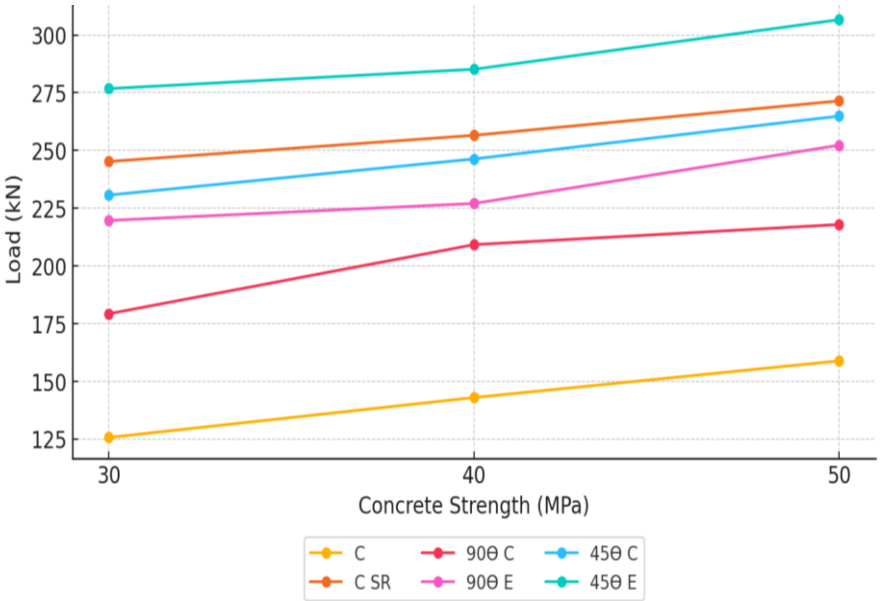

Fig. 8: Effect of concrete compressive strength on load-carrying capacity.

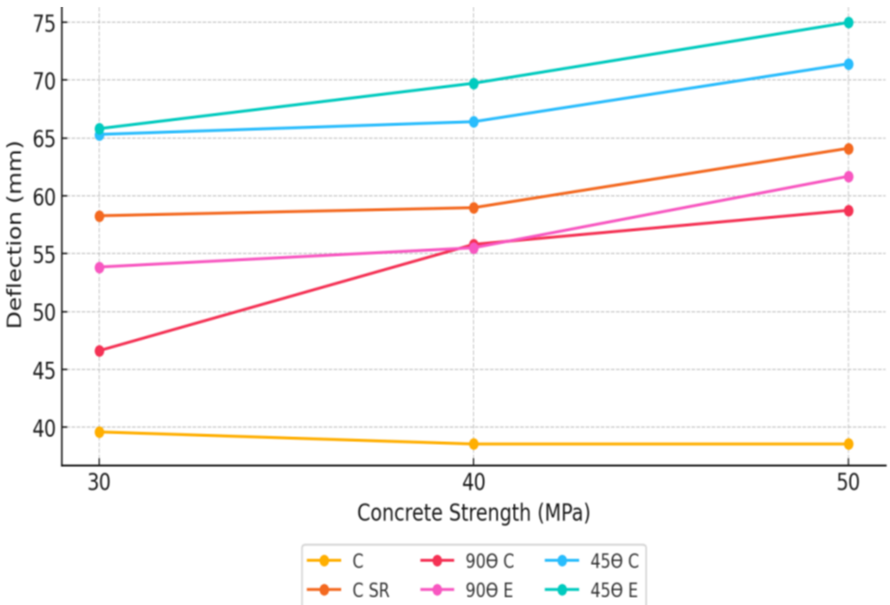

Fig. 9: Effect of concrete compressive strength on deflection value.

4 Conclusion

This study investigated the effects of ETS reinforcement angle, placement location, and recycled plastic aggregate (RPA) content on the structural performance of reinforced concrete beams. The findings underscore the significance of strategic ETS configurations in enhancing load capacity, crack control, and failure behaviour. Among all tested configurations, the 45° edge-placed ETS reinforcement proved to be the most effective, offering a well-balanced combination of increased shear strength, improved crack confinement, and stable failure mechanisms.

1) Validation of experimental findings: The finite element (FE) models demonstrated strong predictive capability, accurately replicating load capacities and failure patterns. Most numerical results deviated by less than 10 % from the experimental values, confirming the robustness and reliability of the simulation approach.

2) ETS Reinforcement angle and shear resistance: The numerical analysis confirmed that 45° inclined CFRP bars outperformed vertically installed (90°) ones in terms of shear resistance. The inclined orientation enabled more efficient distribution of shear stresses, minimizing concentrations and enhancing overall performance.

3) Effect of Bar Diameter on Shear Strength: Increasing the CFRP bar diameter from 6 mm to 10 mm resulted in a notable enhancement in shear strength and stiffness. This effect was especially pronounced in the 45° edge-placed configurations, emphasizing the importance of bar sizing in optimizing ETS performance.

4) Impact of Concrete Compressive Strength: Raising the concrete compressive strength from 30 MPa to 50 MPa led to a significant improvement in beam capacity. This benefit was more evident in beams with 45° ETS reinforcement, where higher concrete strength facilitated better stress distribution and delayed crack initiation.

5) Bond Assumptions in Numerical Models: The numerical models slightly overestimated stiffness due to the assumption of perfect bonding between CFRP bars and concrete. In practice, microcracking, shrinkage, and localized debonding reduce stiffness, highlighting the importance of accounting for realistic bond behavior in future simulations.

Conflicts of interest

The authors declare no conflict of interest.

Funding

The authors declare that no funds, grants, or other support were received during the preparation of this manuscript.

References

[1] KHALIFA, A. C. - HASSAN, M. N. – OKEIL, H. M.: Durability issues in reinforced concrete structures: Causes and preventive strategies. Journal of Materials in Civil Engineering, vol. 32, no. 6, pp. 04020123, 2020.

[2] BENMOKRANE, B. - El-HACHA, R. - CHAALLAL, A.: Use of CFRP bars as reinforcement for concrete structures. Construction and Building Materials, vol. 25, no. 1, pp. 195–200, 2011.

[3] GRACE, M. F. - SALIM, M. R. - ABDOU, R. A.: "Behavior of RC beams strengthened with CFRP laminates in electromagnetic-sensitive environments," Journal of Composites for Construction, vol. 17, no. 4, pp. 560–569, 2013.

[4] YOUNIS, A. - EBEAD, A.: "Embedded through-section (ETS) technique for shear strengthening of concrete beams using CFRP rods," Composites Part B: Engineering, vol. 141, pp. 15–28, 2018.

[5] BOURNAS, D. A. - TSIONIS, G. - TRIANTAFILLOU, T. C.: "Flexural strengthening of RC beams with near-surface-mounted CFRP or steel reinforcement," Journal of Structural Engineering, vol. 135, no. 7, pp. 660–669, 2009.

[6] SOONG, T. T. - MIRMIRAN, M. K.: "Influence of CFRP bar diameter on bond performance and failure mode in concrete," ACI Structural Journal, vol. 113, no. 3, pp. 455–462, 2016.

[7] ZHANG, J. - WU, H. - XING, F.: "Effect of concrete compressive strength on shear performance of FRP-reinforced beams," Construction and Building Materials, vol. 151, pp. 370–380, 2017.

[8] SENNAH, M. N. - GHALI, M. R.: "Size effect in shear of FRP-RC beams," Engineering Structures, vol. 30, no. 12, pp. 3245–3254, 2008.

[9] EL MAADDAWY, T. - SOUDKI, K.: "Effect of beam size on shear strength of concrete beams reinforced with GFRP bars," ACI Structural Journal, vol. 103, no. 2, pp. 267–276, 2006.

[10] KHORASANI, A. M. - MIRMIRAN, A. - IZADI, M.: "Investigation on deep beam shear failure in FRP-RC systems," Materials and Structures, vol. 53, no. 1, pp. 1–12, 2020.
[11] ALSAYED, S. H. - AL-SALLOUM, Y.: "Shear behavior of high-strength concrete beams reinforced with FRP bars," Journal of Materials in Civil Engineering, vol. 24, no. 10, pp. 1232–1241, 2012.
[12] JU, M. - ELGABBAS, F. - ZHU, Y.: "Numerical modeling of shear failure in FRP-reinforced concrete beams using FEA," Composite Structures, vol. 190, pp. 307–319, 2018.
[13] YOO, D. Y. - LEE, S. H. - YOON, Y. S.: "Experimental validation of FEA models for RC beams strengthened with CFRP," Composites Part B: Engineering, vol. 99, pp. 381–397, 2016.
[14] ABAQUS Documentation, Version 6.14, Dassault Systèmes Simulia Corp., Providence, RI, USA, 2017.
[15] KADHIM, M. - FANG, R. Z.: "Finite element study on the size effect of FRP-RC beams under shear," Computers and Concrete, vol. 23, no. 5, pp. 487–500, 2019.
[16] SHAMS, A. - HAWILEH, R. A. - ABDALLA, J.: "Enhanced FEA modeling of shear behavior of RC beams with FRP bars," Engineering Structures, vol. 201, pp. 109793, 2020.
[17] EL-GAMAL, S. M. - EL-SAYED, A. E.: "Calibration of numerical models for predicting shear behavior of FRP-RC beams," Structural Engineering and Mechanics, vol. 69, no. 4, pp. 367–380, 2019.
[18] HAMEED, M. O. - DAUD, R. A.: "Behavior of Fatigue Damaged Reinforced Concrete One-Way Slabs Repaired With CFRP Sheets," *Civil and Environmental Engineering*, vol. 20, no. 1, pp. 364–376, Jun. 2024.
[19] ABED, A. M. O. - DAUD, S. A.: "Flexure Behaviour of Corroded Reinforced Concrete Beams Under Sustained Loads," *Civil and Environmental Engineering*, vol. 20, no. 2, pp. 1162–1173, 2024.
[20] NAJM, I. N. - DAUD, R. A. - AL-AZZAWI, A. A.: "Behavior of Reinforced Concrete Segmental Hollow Core Slabs Under Monotonic and Repeated Loadings," *Structural Monitoring and Maintenance*, vol. 6, no. 4, pp. 269–289, 2019.
[21] AL-ALLAF, M. H. - DAUD, R. A. - DAUD, S. A.: "Nonlinear Finite Element Analysis of Concrete Corbels with Hybrid Reinforcements," *Mechanics of Advanced Materials and Structures*, Oct. 2024, pp. 1–1.
[22] KADER, H. A. - DAUD, S. A.: "Numerical Validation of Reinforced Concrete One-Way Slabs Under Long-Term Loading Using Nonlinear Finite Element Analysis," *Innovative Infrastructure Solutions*, vol. 9, no. 9, art. no. 347, 2024.